Available online at www.sciencedirect.com

SciVerse ScienceDirect

Procedia Engineering 53 (2013) 600 – 606

Procedia Engineering

www.elsevier.com/locate/procedia

Malaysian Technical Universities Conference on Engineering & Technology 2012, MUCET 2012
Part 2 – Mechanical And Manufacturing Engineering

CFD Prediction of Heat and Fluid Flow Through U-Bends Using High Reynolds-Number EVM and DSM Models

M.F. Ghazali[a]* and M.F. A. Rahim[a]

[a]Faculty of Mechanical Engineering, University Malaysia Pahang,
26600 Pekan, Pahang, Malaysia

Abstract

The cooling system of gas turbine blades understanding and improvement is increasing desires for computational techniques which can accurately model the flow field and heat transfer characteristics of blade cooling passage designs under realistic operating conditions. The present study discusses the comparisons between modeling and measuring gas turbine blade-cooling applications of the flow development and heat transfer in a stationary square cross-sectioned U-bend of strong curvature of Rc/D=0.65. A turbulence model of the differential stress model (DSM) is used in combination with three different wall treatments such as a standard form of the wall function (SWF), an analytical wall function (AWF) and a numerical wall function (NWF). The combination of DSM with the numerical wall function (DSM/NWF) has improved markedly the Nusselt number predictions along the outer wall after the bend exit, but did not show any other distinctive predictive advantages over the other DSM models.

Selection and peer-review under responsibility of the Research Management & Innovation Centre, Universiti Malaysia Perlis

Keywords: Gas Turbine Blade, Differential Stress Model, Numerical Wall Function and Nusselt Number

1. Introduction

Gas turbine cooling technology is complex and varies among manufacturers. Blade cooling is accomplished through a combination of external and internal cooling techniques. External film cooling involves blowing compressor bypass air through small holes in the surface of the blade, particularly along the leading edge. Internal cooling involves passing the compressed air through the serpentine channel inside the blade. Figure 1 and Figure 2 shows the common cooling techniques used presently in the industry. Gas turbine cooling technology is complex and varies among manufacturers. Blade cooling is accomplished through a combination of external and internal cooling techniques. External film cooling involves blowing compressor bypass air through small holes in the surface of the blade, particularly along the leading edge. Internal cooling involves passing the compressed air through the serpentine channel inside the blade. Figure 1 and Figure 2 shows the common cooling techniques used presently in the industry.

* Corresponding author.
E-mail address: mfadzil@ump.edu.my

Selection and peer-review under responsibility of the Research Management & Innovation Centre, Universiti Malaysia Perlis
doi:10.1016/j.proeng.2013.02.077

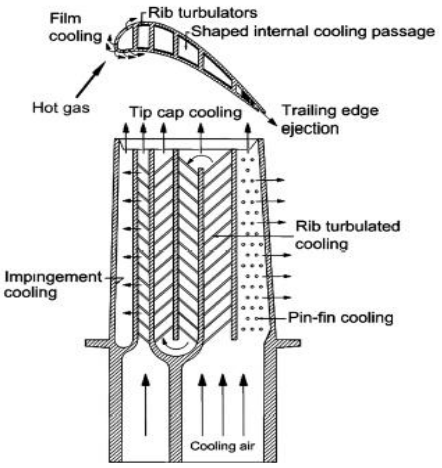

Fig. 1. The schematic of a modern gas turbine blade with common cooling technique.

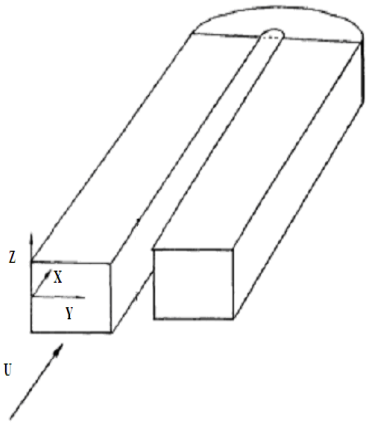

Fig. 2. The geometry of stationary U-bend under investigation.

Both hydraulic and the thermal field within the cooling passage are strongly 3D, very complicated flow features, containing regions of strong acceleration, flow separation and secondary motion. Comprehensive information of the flow and heat transfer in internal cooling can be very essential for design new generation of gas turbine. To gain such information experimentally however can be very difficult and expensive. The other method for producing the details of heat and flow field is to solve the governing equations of the flow and energy numerically. As flows in internal cooling is turbulent, the prediction requires the use of mathematical models of turbulence that reproduce the effect of separation, streamline curvature and rotation on the turbulence field and also to be sensitive to the effects of the Coriolis force. Flow field and heat transfer in real turbine blade-cooling passages is not only affected by the rotation of the blade, but also by the presence of U-bends of strong curvature and heat transfer-enhancing-ribs.

The prediction of flow and heat transfer through passages that are pertinent to blade cooling applications has thus been the subject of numerous investigations [1-5]. Previous work has indicated that the use of standard k-ε eddy-viscosity models (EVM) is somewhat questionable in this flow, due to the model's relatively poor performance in flows involving strong curvature and flow separation. The differential stress model (DSM) of Launder *et.al* [6] is thus tested in the present paper, although k-ε eddy-viscosity models (EVM) results are also shown for comparison. Since there are significant transport effects on the near wall turbulence, standard wall functions are not generally accurate in such a flow. However, the alternative of fully-resolving the boundary layers, using low-Reynolds number turbulence models, can lead to prolonged computing times and expensive in the industrial environment. This is especially true if structured Cartesian meshes are employed, due to the fact that the fine grid near the walls extends into the main flow domain. An alternative approach, explored here, is to use a wall function that can accurately approximate the near wall turbulence transport.

2. Numerical Methods

Simulation of Turbulent Reynolds-averaged Equations for All Mach number of Lien & Leschnizer [7], STREAM is a three-dimensional, fully elliptic, turbulent flow solver which employs a fully collocated (non-staggered), non-orthogonal and body-fitted grid system. It uses the SIMPLE pressure-correction algorithm and the UPWIND, QUICK and UMIST convection schemes. Both steady and unsteady flows can be analysed and mass-weighted averaging can be activated if compressibility effects are significant. Additional equations for total enthalpy or temperature, turbulent kinetic energy, dissipation rate of turbulent kinetic energy and Reynolds stresses are solved subsequently. In the present study therefore, two different turbulence models are considered: the high-Reynolds number linear k-ε model (EVM) [8] and the differential stress model (DSM) [6]. Furthermore, these two turbulence models are used in combination with three different wall treatments: a standard form of the wall function (hereafter denoted SWF) [9], an analytical wall function (denoted AWF) [10], and a numerical wall function (denoted NWF) [11].

The new wall function strategy presented here employs a grid similar to that used with a standard high Reynolds number model treatment (with a large near wall cell) which is used to calculate source terms similar to those approximated in standard treatments (such as the wall shear stress, τ_ω, the average turbulence energy production, $\overline{P}_k$ and average dissipation, $\overline{\varepsilon}$ over the cell). The main difference between numerical wall function and standard treatment is that the numerical wall function does not use any assumed profiles of velocity or length scale. Instead, the turbulence parameters

and mean flow profiles are numerically solved across the near wall cells from solving simplified transport equations using a fine subgrid spanning the wall adjacent control volume and shown in Figure 3.

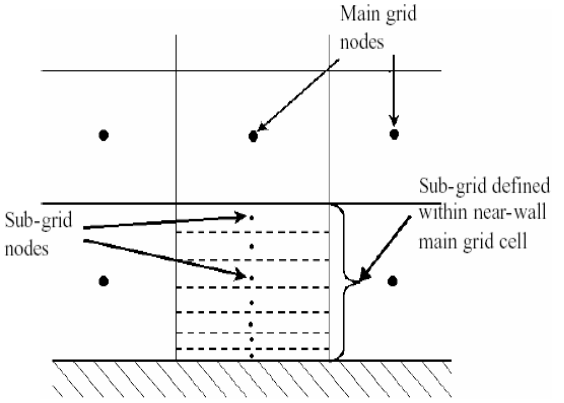

Fig. 3. Subgrid arrangement within near wall main grid control volume [11].

Furthermore, the numerical wall function differs from standard low Reynolds number treatments in that it decouples the numerical solution of the near wall region from that of the main region of the flow domain and also because it does not involve the solution of the pressure correction equation over the subgrid. As a result, numerical wall function does not suffer from slow convergence problems of a full low-Re calculation. In order to obtain a simplified transport equation, a number of assumptions have been made within the subgrid i.e. diffusion parallel to the wall is ignored in comparison to that normal to the wall, only momentum components which are parallel to the wall are solved and also the pressure gradient is assumed to be constant across the near wall grid cell. In 2D Cartesian coordinates the transport equations which are solved across the subgrid.

The wall normal V-velocity in the near wall cell is calculated via continuity across the subgrid as in a conventional boundary layer procedure and is scaled to ensure that the subgrid V-velocity at the outer edge of the subgrid, this phenomenon is shown in Figure 3. It is consistent with the main grid wall normal velocity at that location. The dicretized subgrid transport equations are solved using a tri-diagonal matrix algorithm (TDMA). One sweep of the subgrid TDMA is performed for each main grid iteration, so that the subgrid solution converges as the main grid solution converges. Following each sub grid iteration, wall function parameters are calculated: wall shear stress, average source and sink terms in the k and $\widetilde{\varepsilon}$ equations and wall temperature T_{wall}, or wall heat flux, q_{wall}. These wall function parameters are then applied as source term in the main grid wall adjacent cells following the conventional wall function approach. Low-Reynolds-number terms are included in the equations solved in the main grid, so that near wall cell size become small. Moreover, in a stagnant flow region where turbulent Reynolds numbers are locally small even in the primary grid, the turbulent model is still able to cope.

3. Computational Grids and Boundary Conditions.

Figures 4(a) and 4(b) shows a body fitted grid consisting of 103 planes in the streamwise direction, 34 nodes across the duct and 18 from the symmetry plane to the top wall. Along the streamwise direction (x-direction) 103 planes were divided into four different regions: 13 were used in the upstream tangent, 15 in the first half of U bend, 25 in the second half of the U bend and the remaining 50 in the downstream tangent. A symmetrical non uniform grid is employed along the y- and z-direction which produced a fine distribution of grid nodes near the north-south and top bottom wall. Furthermore, the grid spacing expands linearly with the distance from the wall surfaces to the middle of the cross-section. In general, the conditions at symmetry boundary are: i) no mean flow rate across the boundary and ii) no scalar flux across the boundary. In the implementation, normal velocities are set to zero at a symmetry boundary and the value of all other variables at the boundary are set to those at the nearest cell inside the computational domain. Moreover, the discretised transport equations the zero flux condition normal to the boundary is applied by setting the appropriate coefficient to zero. In all cases, a pre-calculation in a straight duct was carried out in order to generate fully developed, upstream inlet boundary condition and thermal conditions.

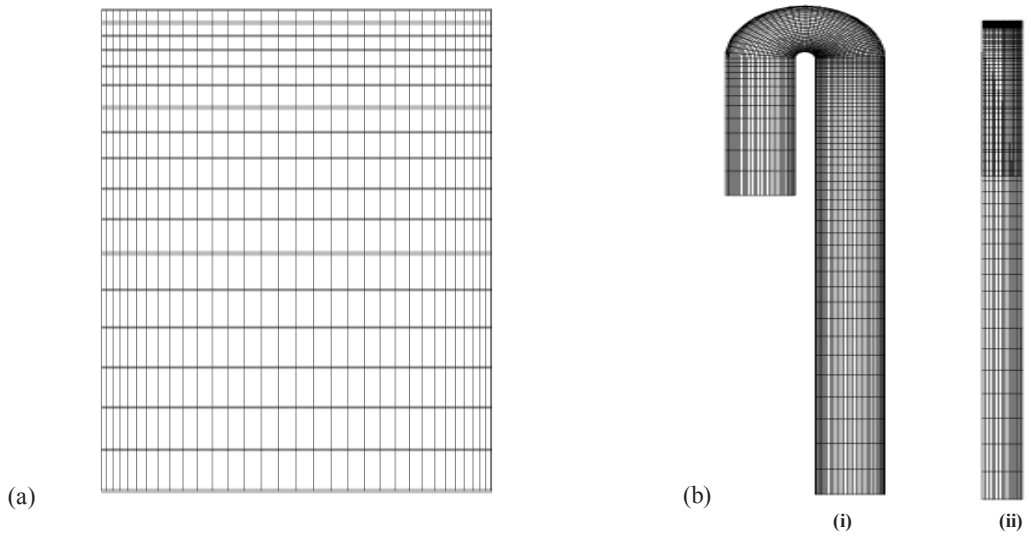

Fig. 4. Grid Distribution of (a) Cross section (34x18) (b) Streamwise direction ((i) 104x34, (ii) 104x18)

4. Results and Discussion.

Footnotes For experimental data, both for flow field [12] and heat transfer [13] with which the present computational results are compared were performed at UMIST. The radius of curvature to hydraulic diameter ratio, R_c/D is 0.65 and the diameter of the square cross sectioned bend is 50mm. The flow Reynolds number based on the streamwise bulk velocity and the hydraulic diameter, is 100,000 for the mean flow measurements and 95,000 for the heat transfer experiment. Laser Doppler Anemometry (LDA) was used to obtain the flow measurement. The upstream straight section of the model was about 9D which relatively long enough to allow the flow at the bend entry to be practically developed. The downstream straight section was 11D. Water was used as the working fluid under nearly constant temperature, 20ºC. The number of control-volume cells is 104 x 34 x 18.

Comparisons of the local Nusselt number contours are shown in Figure 5a and 5b. The measurements show that, in the upstream section, the Nusselt number levels along both walls are fairly uniform with the averaged value being about 225. All predictions agree qualitatively with the data on these general features except that, near the duct corners, all models show a reduction in the Nusselt number and thus lower than measurement there. Into the bend, the overall level of the measured Nusselt number starts to increase as the flow accelerates along the outer wall. DSM/SWF and EVM/SWF predicts that the increase in Nusselt number near the outer wall starts further downstream compared to other models, probably due to standard wall function equation not able to respond to the effect of streamwise pressure gradient. The Nusselt number continues to increase along the centreline of the outer wall, caused by the secondary motion and reaching a maximum at about halfway down the end wall. At this location, the cool fluid from near the duct centre impingement along the centerline of the outer wall. As a result, this fluid heats up as it moves out to the corner regions, leading to reduction in the heat transfer coefficient in the two corners. It is observed that, the DSM models clearly improves the prediction, particularly in the vicinity of the outer corner regions, where EVM models had considerably over-estimate the heat transfer levels about 40%. In the downstream region, the level of Nusselt number near the outer wall is predicted to rise. At three diameters downstream of the bend which is a region of streamwise acceleration, the measurement indicate that heat transfer coefficients generate a maximum value more than double that prevailing upstream, the predictions of all suggest a maximum location about one diameter downstream with wider region than measured ones. At this position, the Nusselt number is seriously over-estimated by all models employed more than 100%. One possible explanation is difficulty in capturing so-called relaminarization [14] that occurs along the outer wall, during process of flow acceleration. Beyond this point, as the flow along the outer wall starts to slow down and the turbulence levels begin to reduce, the high Nusselt number level also start to fall. The EVM's and DSM's prediction become very much similar and in good agreement with the data, but the predicted values not as far as in the experimental data. Moreover, after six diameters downstream of the bend, the corresponding experiment data shows that the Nusselt number is still more than 50 percent higher than upstream. DSM/NWF and EVM/NWF results are slightly closer agreement with the data at this location.

On the other hand, along the inner wall, the Nusselt number levels rise very rapidly after the bend exit, similar to those along the outer wall. In contrast to the measured distribution along the outer wall, along the inner wall, the Nusselt numbers

in the corner regions are higher than those the centerline. From the bend exit, about one diameter downstream, all models returned similar predictions which show that the values of Nusselt numbers at the symmetry line higher than those near the top wall. However, the measurement data seem to suggest otherwise. About two diameters downstream of the bend exit, which is very close to reattachment point, the Nusselt numbers reaching their maximum values. At this region, the value of Nusselt number predicted by all models considerably under-estimated. As fluid moves toward the duct centre, it is heated and also slowed down by the inner wall, causing a strong reduction in wall heat transfer. At about three diameters downstream of the bend the corresponding experimental data suggest variation in Nusselt number between the centerline and the corner regions at the inner wall is about 60 percent. All the predictions agree qualitatively with the data on the features. Further downstream, the Nusselt number levels along the inner wall start to fall. Moreover, even after six diameters downstream from the bend exit, as for the outer wall, the Nusselt number levels still are considerably higher than the upstream region. At this location, all models tested substantially under-estimate the Nusselt numbers.

Figure 5 shows streamwise distributions of side averaged Nusselt number on the inner and outer walls of the bend. The higher measured levels of the heat transfer in the upstream section are probably due to the flow which is not having been fully developed at the entry. With attention first focused on the inner wall, it is seen that, both EVM and DSM models are similar and slightly lower than corresponding experimental data. This predictive deficiency is probably caused by the differences in defining the reference temperature scale and in determining the inlet flow conditions between experiment and computation. Along the inner wall the within the bend experimental data are not available. In the second half of the bend and in downstream region, The DSM/NWF model returns maximum average Nusselt numbers at about two diameters downstream, and this brings the prediction closer to the measurement, while other models have their maximum average Nusselt number occur at about three diameters downstream. The peak value of DSM/NWF model is excellent agreement with the data. Further downstream, the averaged Nusselt number along the inner wall start to diminish. At this stage, all models generate similar averaged Nusselt numbers, though DSM/SWF model and DSM/AWF model are in good accord with the data. These results clearly show that the averaged Nusselt numbers are consistent with those for local Nusselt numbers as shown earlier.

In the vicinity of the bend, the predicted averaged Nusselt number starts to increase towards the outer side, as the measured ones do. The measured data touch their maximum average Nusselt numbers value about 440 at three diameters downstream of the bend exit. About one diameter downstream of the bend exit, predicted reaches their peak value of average Nusselt number. At this region, the computations return greatly over-predicted of average Nusselt number about 1.72, 1.52, 1.45, 1.59, 1.42 and 1.36 times higher than experimental data for the EVM/NWF model, EVM/AWF model, EVM/SWF model, DSM/NWF model, DSM/AWF model and DSM/SWF model, respectively. Further downstream of the bend exit, average Nusselt numbers are reduced somewhat from the peak value. The DSM's and EVM's predictions are very much similar. Moreover, it is seen that, good agreements are achieved between the predictions and the measurements, though, further downstream, it is slightly worse.

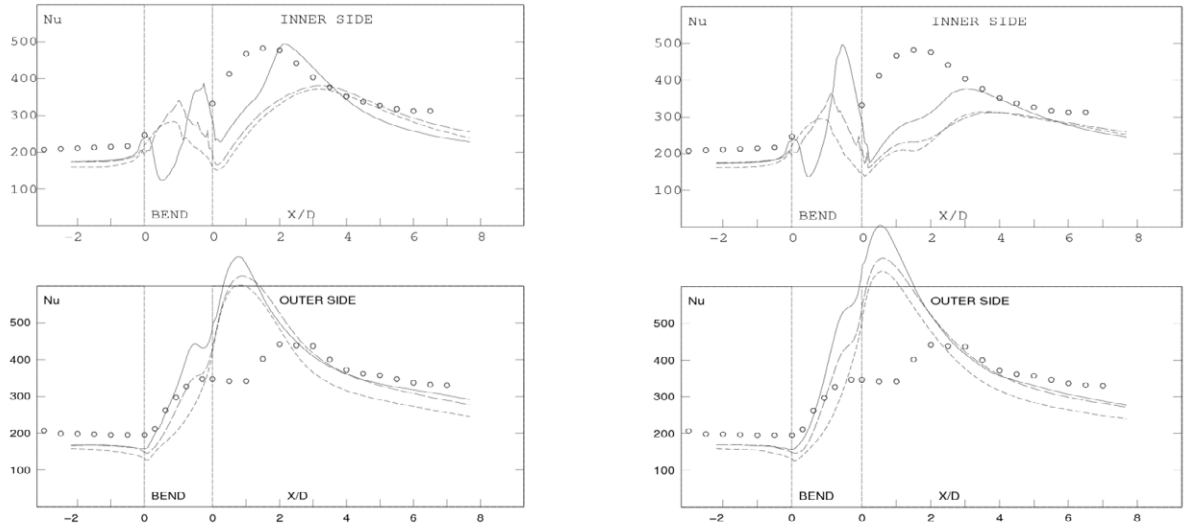

dashed curve: DSM/AWF, solid curve: DSM/NWF, thin dashed curve : DSM/SWF
open circle: UMIST exp. [13]

Fig. 5. Comparisons of side-average Nusselt number distributions for (a) DSM and respective wall functions (b) EVM and respective wall functions.

whether more elaborate treatments of DSM/NWF model, can improve the prediction in such manner. In the previous prediction of DSM/NWF model, the subgrid nodes were divided into 20 thin slices, while in the new version of DSM/NWF model (hereafter denoted DSM/NWF2), the subgrid nodes were divided into 40 thin slices. The DSM/NWF2 model is expected to work better in separation flow. Both approaches were tested and compared with the experimental data as shown in Figure 6. The introduction of the more elaborate wall function, WF2, have improved the prediction of the average Nusselt number levels returned by DSM/NWF along the outer wall at the bend exit by 24%. However, after three diameters downstream of the bend exit DSM/NWF model performed better than DSM/NWF2 model but the predicted values still lower than the experimental data. Along the inner wall, where the flow separates at the bend exit, the two models's predictions are very much similar. Both models under-estimated the average Nusselt numbers level from the bend exit up to two diameters from the bend exit. Generally, therefore, the above comparisons suggest that, there is no significant different between DSM/NWF2 model and DSM/NWF model. The most important feature of the heat transfer predictions of DSM/NWF2 is that, along the outer wall at the bend exit the discrepancy between prediction and the measurement data of average Nusselt numbers level has been reduced from about 56% to about 32%. In addition, the DSM/NWF2 calculation took longer time compared to DSM/NWF calculation.

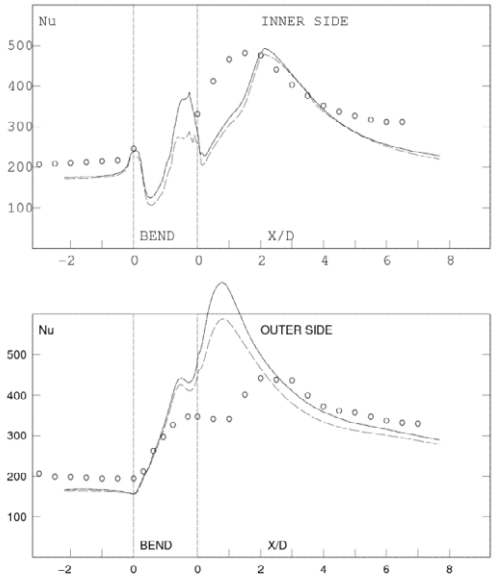

dashed curve: DSM/NWF2, solid curve: DSM/NWF, open circle: UMIST exp. [13]

Figure 6: Comparisons of side-average Nusselt number distributions for 40 thin slices

5. Conclusions

The comparisons presented here establish how effective high-Reynolds-number models are in computations of complex, three dimensional flows that are relevant to blade-cooling applications. The cases considered only for stationary blade which contain important feature encountered in blade-cooling passages, namely strong curvature. While agreement with experimental data cannot be said to be complete, the second-moment closure (DSM) consistently produced more realistic flow and heat transfer predictions than the widely used effective-viscosity model (EVM). This confirms the findings of earlier studies that in complex flows with streamline curvature and flow separation, the anisotropy of the turbulence field strongly influences the flow and thermal development. At least some of the remaining differences, between the predictions and the experimental data are caused by the use of the wall function approach. The development of more refined wall functions as presented here may be a more promising route to follow. On the other hand, more elaborate DSM with numerical wall function (DSM/NWF2) has improves markedly the Nusselt number predictions, but did not show distinctive predictive advantages over the other DSM models.

References

[1] Iacovides, H., Launder, B.E. and Li, H.Y., 1996, *"The computation of flow development through stationary and rotating U-ducts of strong curvature"*, Int. J. Heat Fluid Flow Vol.17, pp. 22-33.
[2] Bonhoff, B., Tomm, U., Johnson, B.V. and Jennions, I., 1997, *"Heat transfer predictions for rotating U-shaped coolant channels with skewed ribs and with smooth walls"*, Paper 97-GT-162, ASME, 1997.
[3] Iacovides, H., Launder, B.E., and Li, H.Y., 1996 *"Application of a reflection-free DSM to turbulent flow and heat transfer in a square-sectioned U-bend"*, Exp. Thermal and Fluid Science, Vol.13, pp. 419-429.
[4] Okita, Y., and Iacovides, H., 2003 *"Comparisons of high-Reynolds-number EVM and DSM models in the prediction of heat and fluid flow of turbine blade cooling passage"*, ASME J. Turbomach., Vol.125 , pp. 585–597.
[5] Suga, K., 2003, *"Predicting turbulence and heat transfer in 3D curved ducts by near wall second moment closure"*, Int. J. of Heat and Mass Transfer, Vol. 46, pp. 161-173.
[6] Launder, B. E., Reece, G. J., and Rodi, W., 1975, ''Progress in the Development of a Reynolds Stress Turbulence Closure,'' J. Fluid Mech., 68, pp. 537– 566.
[7] Lien, F.S. and Leschziner, M.A., 1994a, *"A General, non-orthogonal, collocated, finite volume algorithm for turbulent flow at all speeds incorporating second-moment turbulence-transport closure, Part: Computational Implementation"*, Comput, Methods Appl. Mech. Engrg., Vol. 114, pp. 123-148.
[8] Launder, B.E. and Sharma, B.I., 1974, *"Application of the energy-dissipation model of turbulence to the calculation of flow near a spinning disc"*, Lett. In Heat mass Transfer, Vol. 1, pp. 131-138.
[9] C. C. Chieng and B. E. Launder, 1980. On the calculation of turbulent heat transport downstream from an abrupt pipe expansion. Numerical Heat Transfer, 3:189–207,
[10]Gerasimov, A.V., 1999, *"Modelling mixed convection in vertical pipes using wall functions"*, MSc Dissertation, Department of Mechanical Engineering, UMIST, Manchester, UK.
[11]Gant, S.E., 2002, *"Development and application of a new wall function for complex turbulent flows"*, PhD Thesis, UMIST, Manchester, UK.
[12]Cheah, S.C., Iacovides, H.., Jackson, D.C. and Launder, B.E., 1996, *"LDA investigation of the flow development through rotating U-ducts"* ASME J. Turbomach., Vol.118, pp. 590–596.
[13]Iacovides, H., Jackson, D.C., Kelemenis, G. and Launder B.E., 2000, *"The measurement of local wall heat transfer in stationary U-ducts of strong curvature, with smooth and rib roughened walls"*, ASME Journal of Turbomachinery, Vol 122, pp 386-392.
[14]Li. H.Y., 1995, *"The computation of 3D-turbulent flows in curved and rotating ducts"*, PhD Thesis, Dept. of Mechanical Engineering, UMIST, U.K.